Influence of the anion on the electrical conductivity and glass formation of 1-butyl-3-methylimidazolium ionic liquids

Jan Leys,[1, a)] Ravindran Nair Rajesh,[1] Preethy Chirukandath Menon,[1] Christ Glorieux,[1] Stéphane Longuemart,[2] Peter Nockemann,[3] Michael Pellens,[3] and Koen Binnemans[3]

[1)] *Laboratorium voor Akoestiek en Thermische Fysica, Departement Natuurkunde en Sterrenkunde, Katholieke Universiteit Leuven, Celestijnenlaan 200D – Po. Box 2416, B-3001 Leuven, Belgium*

[2)] *Univ. Lille Nord de France, F-59000 Lille, France; ULCO, LDSMM, F-59140 Dunkerque, France; CNRS UMR 8024, F-59140 Dunkerque, France*

[3)] *Laboratorium voor Coördinatiechemie, Afdeling Moleculair Design en Synthese, Departement Chemie, Katholieke Universiteit Leuven, Celestijnenlaan 200F – Po. Box 2404, B-3001 Leuven, Belgium*

(Dated: 18 May 2010)

Six ionic liquids based on the 1-butyl-3-methylimidazolium cation have been studied. As anions Cl^-, Br^-, I^-, $[NCS]^-$, $[N(CN)_2]^-$, and $[BF_4]^-$ were selected. The electrical conductivities were determined between 173 and 393 K based on impedance measurements in the frequency range from 0.1 to 10^7 Hz. The electrical conductivity increases, whereas the glass transition temperature, the fragility, and the low temperature activation energy decrease with increasing anion size. The results can be understood from the changing anion-cation interaction strength with changing anion size and from the energy landscape interpretation of the glass transition dynamics.

PACS numbers: 64.70.pm, 66.10.Ed, 72.80.-r

Keywords: Glass transitions in liquids, Ionic conduction, Conductivity of specific materials

[a)] Post-doctoral researcher for Research Foundation – Flanders (FWO); Email address:jan.leys@fys.kuleuven.be

I. INTRODUCTION

Ionic liquids (ILs) are organic salts with a low melting point, typically below 100°C. The current interest[1] in their properties stems from their potential in electrochemical and catalytical applications. In particular their high electrical conductivity and very low vapor pressure are advantageous, as well as the fact that by proper design their physical and chemical properties can be tuned for specific applications. Due to the large number of possible cation–anion combinations, it is of great interest to understand how the properties of newly synthesized ILs can be predicted from the structure of the molecule, in order to choose suitable candidates for a given application.

One of the properties of ILs, which is of indirect importance to those applications, is their tendency to form supercooled melts and glasses at low temperatures. The study of the glass transition is an important topic in soft condensed matter research. Whereas the phenomenology of the behaviour is well known, the theoretical understanding and modelling is far from complete. Information about how the molecular properties of the glassforming molecule influence the glass transition may contribute to a better understanding of this phenomenon. ILs are interesting candidates for this type of research, as a rich variety of them is available and many of them reach a glassy state upon cooling. Rivera *et al.* have shown, using broadband dielectric spectroscopy and depolarized light scattering, that ILs behave like typical glassforming liquids[2,3]. Also other ILs[4] and properties, like solvation dynamics[5], diffusion coefficients[6,7], structure[8] and heat capacity[9] have been studied at temperatures towards the glass transition.

Some systematic work is available concerning both the glass formation and electrical conductivity in ILs. In particular for the subclass of protic ILs (which includes many of the commonly studied ILs), Angell and coworkers have discussed relations between molecular structure, glass formation, phase transitions and transport properties[10–14]. They conclude that the mechanisms involved are quite subtle, including in their reasoning also the formation energies and the acidity or basicity of the acid and base from which protic ILs can be formed. Also other researchers have investigated protic ILs[15,16].

Systematic searches have also been performed by other researchers. In three successive papers of the same group, ionic liquids for which the anion[17], the cation alkyl chain length[18] and the cation[19] were varied, were studied with multiple experimental techniques, including

electrical conductivity measurements. The focus of these works was on ILs with perfluorinated anions. A work also including changing anions with a fixed cation[20] shows that for $[C_2mim]Br$ and $[C_2mim]I$, the electrical conductivity is quite similar; further it also compares well to the values given for $[C_2mim][TfO]$ and $[C_2mim][Tf_2N]$ (where $[TfO]^-$ stands for trifluoromethanesulfonate and $[Tf_2N]^-$ for bis(trifluoromethanesulfonyl)amide). The results were mainly obtained at room temperature and above.

In previous work[21], we have determined the electrical conductivity of a substantial number of compounds, looking for tendencies in the electrical conductivity, its temperature dependence and the glass transition temperature with changing ion features. We studied the properties of the 1-alkyl-3-methylimidazolium tetrafluoroborate series ($[C_nmim][BF_4]$), where the length of the alkyl chain n was varied from 2 to 11. Also a short series of 1-hexyl-3-methylimidazolium with different anions was included. We found that the values of the electrical conductivity and the fragility for 1-hexyl-3-methylimidazolium bromide ($[C_6mim]Br$) were significantly different from those of the other compounds, and we linked this to the presence of hydrogen bonding between the hydrogen atoms on the imidazolium ring and the bromide ion[21].

In the present work, we continue to study the same type of ILs —imidazolium-based ILs with the possibility to form a hydrogen bond— but this time in a more systematic way. The cation was fixed to 1-butyl-3-methylimidazolium, $[C_4mim]^+$, whereas the anion was varied.

We have structured this paper as follows. Details of the experimental setup are discussed in Sect. II. The results and the analysis of the data are given in Sect. III, with specific attention for the electrical conductivity (III A), the parameters related to the glass formation (III B) and a comparison of different models for the temperature dependence of the electrical conductivity (III C. These results are discussed in Sect. IV, leading to a conclusion given in Sect. V.

II. EXPERIMENTAL DETAILS

We studied six ionic liquids based on the 1-butyl-3-methylimidazolium cation $[C_4mim]^+$. The anions selected were chloride (Cl^-), bromide (Br^-), iodide (I^-), thiocyanate ($[NCS]^-$), dicyanamide ($[N(CN)_2]^-$), and tetrafluoroborate ($[BF_4]^-$). The first three of them, Cl^-, Br^-, and I^-, are halide ions. The two larger anions $[NCS]^-$ and $[N(CN)_2]^-$ are called pseudo-

halide ions, as their properties show similarities with those of the genuine halides. For comparison, the "model IL" [C_4mim][BF_4] was included in the survey. All six compounds were obtained from IoLiTec (Ionic Liquids Technologies GmbH & Co. KG, Denzlingen, Germany).

Two series of electrical conductivity experiments were conducted. In the first series, the ILs were measured as received. In the second series, additional drying was performed. Prior to measurement, all the samples were dried with the Schlenk technique at 105℃, and then stored and packaged for transport to the experimental setups in a glove box under argon atmosphere. The samples were then transferred in the closed measurement cells under dry nitrogen atmosphere.

The water content of the samples was determined by means of a Mettler Toledo Coulometric Karl Fischer Titrator (model DL39). Specifications for the measured ILs are summarized in Table I. The water concentration is given in ppm (mass concentration). 100 ppm typically corresponds to a molar concentration in the order of 0.1% for ILs of this molecular weight.

Dielectric experiments have been performed with the same equipment and under the same circumstances as described earlier in Ref. 21. A Novocontrol Alpha dielectric analyzer and Quatro temperature controller were used to obtain complex impedance data from 0.1 to 10^7 Hz for temperatures ranging from 173 to 393 K. The sample was placed in an airtight stainless steel parallel plate capacitor. The temperature was controlled by a nitrogen flow.

The temperature range for [C_4mim][NCS] was limited to 30℃, because this compound turned out to be unstable at higher temperatures. In the first run, a reaction involving the sample resulted in a black liquid and caused the IL to leak out of the measurement cell. During the drying process, white fumes were formed that were not due to water vapour, but might have been decomposition products.

From the dielectric results, the electrical conductivity σ was obtained from the region in the imaginary part of the complex dielectric permittivity ($\epsilon^* = \epsilon' - i\epsilon''$) where the slope of $\log \epsilon''$ versus $\log \omega$ is equal to -1. The intercept of this straight line is the dc-conductivity, since for the (idealised) case of a compound with purely Ohmic conductivity:

$$\epsilon'' = \frac{\sigma_0}{\epsilon_0 \omega} \ , \tag{1}$$

with ϵ_0 the permittivity of vacuum and ω the angular frequency of the applied measuring electrical field. A more extensive discussion of this approach can be found in Ref. 21.

TABLE I. Properties of the studied ionic liquids.

Compound	Material	Amount	Method
$[C_4mim]Cl$	Nominal	99%	
	$[C_4mim]$	99.88%	IC[a]
	Water	89 ppm	KF[b]
$[C_4mim]Br$	Nominal	99%	
	$[C_4mim]$	98.83%	IC
	Water	68 ppm	KF
$[C_4mim]I$	Nominal	>98%	
	Water	61 ppm	KF
$[C_4mim][NCS]$	Nominal	>98%	
	$[C_4mim]$	98.83%	IC
	[NCS]	99.74%	IC
	Cl	0.26%	IC
	Water	98 ppm	KF
$[C_4mim][N(CN)_2]$	Nominal	>98%	
	$[C_4mim]$	99.53%	IC
	$[N(CN)_2]$	99.29%	IC
	Cl	0.71%	IC
	Water[c]	430 ppm	KF
	Water	58 ppm	KF
$[C_4mim][BF_4]$	Nominal	99%	
	$[C_4mim]$	99.8%	IC
	$[BF_4]$	99.99%	IC
	Cl	0.01%	IC
	Water[c]	150 ppm	KF
	Water	22 ppm	KF

[a] Ion chromatography, performed by Iolitec

[b] Karl Fischer titration

[c] Data for the undried sample, supplied by Iolitec

The glass transition temperature T_g was obtained from a standard DSC experiment. Aluminium sample holders were placed in a TA Instruments Q1000 DSC. Two measurements have been performed. First the samples were measured without any treatment (the transport to and transfer into the DSC apparatus involved some steps where the samples were shortly exposed to the atmosphere). For the second run, the samples were dried *in situ* by heating them in a pierced pan to 70 or 80℃ under nitrogen atmosphere for two hours directly prior to the measurements. T_g was determined as the temperature of the inflection point of the heat flow vs temperature curve in a 10 K/min heating run.

Because of the used experimental procedures, two series of impedance and T_g measurements are obtained: at an unknown but still reasonably low water content and at the lower water content reported in Table I. It was observed that the conductivity in the dry samples was lower than in the undried samples, by 10-30% in the liquid phase and by 2-3 orders of magnitude in the crystalline phase. T_g dropped by 5-20 K for the samples with higher water content. In the following, only data for the dried samples have been used.

III. RESULTS

A. Electrical conductivity

In Table II our results for the electrical conductivity are compared to literature values and to viscosity values.

Literature values for the electrical conductivity of these ILs have not often been reported: for $[C_4mim]Br$ and $[C_4mim][NCS]$ we were even unable to find literature data. Where there are values available, they were read from the figures in the publications, resulting in a substantial error. Considering this limitation, the values for $[C_4mim]I$ and $[C_4mim][N(CN)_2]$ are comparable with the literature values. In the same respect, the value at 20℃ for $[C_4mim]Cl$ is alike, but the 2-order of magnitude deviation at lower temperature may reflect the difference in water content between the two samples. When the complete curve of Ref. 3 is compared to our results, one sees a clear difference in T_g. This circumstance easily leads to large differences of the actual values at fixed temperatures, although the physics of the system is clearly the same.

No room temperature data for the viscosity of $[C_4mim]Cl$ and $[C_4mim]Br$ were found,

TABLE II. Comparison of the conductivity and viscosity values for a number of the studied ionic liquids at different temperatures.

		σ [S/m]				
Compound	T [°C]	This work	Literature	Reference	Viscosity [mPa s]	Reference
$[C_4mim]Cl$	20	0.0023	0.0050	3		
	-20	$8.4 \cdot 10^{-7}$				
	-21		$1.4 \cdot 10^{-5}$	3		
	-40	$4.1 \cdot 10^{-10}$				
	-41		$6.9 \cdot 10^{-8}$	3		
	80				146.8	22
$[C_4mim]Br$	20	0.0077				
$[C_4mim]I$	20	0.028	0.058	20		
	25				1110	23
	75	0.71				
	76		1.2	20		
	117		3.1	20		
	120	2.5				
$[C_4mim][NCS]$	20	0.42			54	24
$[C_4mim][N(CN)_2]$	20	0.94				
	25		1.09	25	29.3	25
	70		2.85	25	6.9	25
$[C_4mim][BF_4]$	20	0.32				
	25		0.35	26	180	26
					104.2	7

as their melting points are much higher than room temperature. As far as the comparison allows, the observation that the conductivity is inversely proportional to the viscosity (Walden rule, see Sect. IV) can be qualitatively observed from the data in Table II.

In Figure 1, the conductivity values for the three cooling runs for each sample are included. As a first observation, we see that the relative order for the value of the electrical conductivity

remains the same for the entire temperature range, and that this order is that of increasing anion size: the ILs with larger anions are more conductive. $[C_4mim][N(CN)_2]$ has one of the higher values available in literature with 0.94 S/m at room temperature (293.15 K).

The figure shows that all six compounds have a pronounced curved, so called fragile, behaviour, as seen in many glassforming substances. Moreover, no evidence for crystallization can be seen before the conductivity contribution to the spectrum moves out of the experimentally accessible frequency window. There are two compounds which show some particular behaviour.

In two of the three cooling runs, $[C_4mim]Cl$ follows the "normal" behaviour, but in one of them, it goes to a state with a higher conductivity compared to the "normal" one. We are unsure about the nature of this state, and think that is probably not a crystalline phase, since on heating the same trajectory is followed, reaching again the fluid state with a visible melting transition at a temperature much below the standard melting point of 70°C[22]. Similar behaviour has been observed in the undried $[C_4mim]Cl$ and in the undried $[C_4mim]Br$.

The temperature dependence of $[C_4mim][N(CN)_2]$ shows a clear change near -40°C: the VFT-like curved behaviour at higher temperatures is replaced by an Arrhenius (straight line) behaviour at lower temperatures. Yoshida *et al.* report a crystallization at -35°C[25] and Fredlake *et al.* report this at -25°C[27]. But, on the basis of the same argumentation as above, crystallization is a doubtful scenario. There is no sharp step at this temperature, as one would expect at a crystallization, and the heating run follows the same trajectory as the cooling run.

In both cases, the temperature at which these changes occur corresponds roughly to the temperature at which several models predict a change in the dynamics of the glassformers ($1.3T_g$, see next section). However, some questions that remain for such an interpretation are the following. Why does it not occur in $[C_4mim]Cl$ in all cooling runs? And why does it depend on the water content, as seen in $[C_4mim]Cl$ and $[C_4mim]Br$? In contrast, in $[C_4mim][N(CN)_2]$, the change is independent of the water content.

B. Glassforming behaviour

In order to get quantitative information about the glassforming behaviour of the ILs, we have performed fits of the conductivity data to the Vogel–Fulcher–Tammann (VFT) equation. This phenomenological equation is widely used to describe data of glassforming systems, since it can reproduce the curvature in the Arrhenius plot that is typical for many glassformers. The VFT-equation has been used here in the form

$$\sigma(T) = \sigma_\infty \exp\left(-\frac{B}{T - T_0}\right), \tag{2}$$

where σ_∞ is the high temperature limit of the conductivity, B is a fitting parameter controlling the curvature (which can also be viewed as the high temperature activation energy of the process underlying the conductivity), together with T_0, the Vogel temperature that typically lies a few tens of degrees below T_g. Various interpretations of T_0 can be found in literature (see e.g. Ref. 28), one of them being that T_0 is the temperature at which the relaxation time would diverge.

Because of the shape of the VFT-curve, the determination of T_0 requires that there are experimental data points near T_0. Though it is impossible to experimentally reach the dynamics around T_0 (the measurement time would become irrealistically long), in this work (and also our previous work[21]), we have obtained data at temperatures that in many systems nearly reach as low as T_g, in contrast to much of the earlier work.

In Figure 1 the data are presented that have been used later on for the Vogel–Fulcher–Tammann fits. The data points at the highest temperatures have rather large error bars because the conductivity region in the spectra had shifted to high frequencies, and only a few points could be used to extract σ. At low temperatures, an analoguous argument applies: the conductivity-dominated region shifts to low frequencies and out of our experimental window.

It seems possible, at first sight, to fit the entire temperature dependence with a single VFT expression. However, a more careful view on the data shows that this is not always the case. Therefore, we have performed, where possible, VFT-fits over three temperature ranges. For all three ranges, only data points in the cooling runs were included.

Full liquid range: the entire temperature range over which the sample is measured and over which it clearly is liquid. This corresponds, except for $[C_4mim][N(CN)_2]$ (be-

low -38℃ is excluded) and [C_4mim]Cl (the deviation is excluded), to the data points depicted in Fig. 1.

Stickel plot range: for a data set expected to show VFT behaviour one can calculate the derivative

$$\left(\frac{\mathrm{d}\ln\sigma}{\mathrm{d}T}\right)^{(-1/2)} = \frac{1}{\sqrt{B}}T - \frac{T_0}{\sqrt{B}} \ . \tag{3}$$

Thus on this type of derivative plot, a VFT dependence should shows as a straight line with non-zero intercept. (An Arrhenius dependence would show as a straight line with zero intercept, since it corresponds to $T_0 = 0$.) This derivative can be used as a very sensitive test to distinguish multiple dynamic regimes that should be described with different sets of VFT parameters[29]. In this work, a temperature region has been selected from the lowest temperatures up that, according to this derivative plot, is described by a single set of VFT parameters.

"$1.3T_g$" range: it is seen that at a temperature between $1.15T_g$ and $1.3T_g$ some change takes place in the dynamical behaviour of the glassformer[28]. This temperature corresponds e.g. to the critical temperature of the mode coupling theory[30], or the temperature where dynamic heterogeneity becomes visible, or to the decoupling temperature for rotational and translation dynamics[31,32].

The "strength" of a glassformer is (inversely) quantified via the fragility m, the slope of $\log\tau$ versus $1/T$ evaluated at T_g, where τ is a parameter reflecting the relaxation dynamics, typically a relaxation time obtained from dielectric or mechanical spectroscopy or the viscosity. In this work only the electrical conductivity is available, but since it is related to the viscosity of the system (via e.g. the Walden rule, Eq. (11), given below), VFT parameters extracted from σ are meaningful quantities. The calculation of the fragility is performed according to[33]

$$m = \left.\frac{\mathrm{d}\log_{10}\sigma^{-1}}{\mathrm{d}\left(\frac{T_g}{T}\right)}\right|_{T=T_g} = \frac{B}{\ln 10}\frac{T_g}{(T_g - T_0)^2} \ . \tag{4}$$

This definition shows that m is proportional to the effective activation energy at T_g, with $1/T_g$ as the proportionality constant.

The results of this analysis have been summarized in Table III. Some relevant parameters are given about the fitting range: the temperature limits and the number of included data

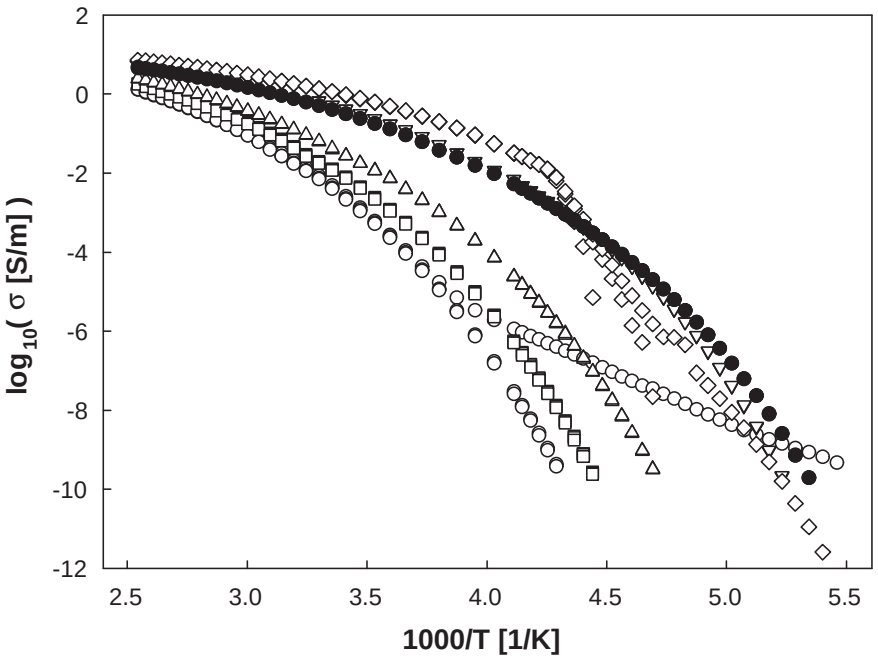

FIG. 1. Arrhenius plot for the electrical conductivity versus inverse temperature for the six ILs. ○: $[C_4mim]Cl$; □: $[C_4mim]Br$; △: $[C_4mim]I$, ▽: $[C_4mim][NCS]$; ◇: $[C_4mim][N(CN)_2]$; ●: $[C_4mim][BF_4]$.

points. The data were only taken from cooling runs. The errors quoted are the fitting errors that do not reflect systematic experimental errors, since the latter ones are much smaller. The errors on the fitting parameters have been calculated on the basis of a most squares approach[34], which takes covariances between fitting parameters into account.

When interpreting the fragility parameters in Table III, one must first be aware of some caveats. First of all, the values for the fragility obtained from the fits in the low temperature ranges (Stickel range and $1.3T_g$ range) are more relevant than that over the full fluid range. The values of the VFT parameters strongly depend on the "choice" of T_0, and T_0 (the temperature at which the relaxation property will diverge) can be determined more accurately (this mainly means: with a more physically relevant value) if there are more data points near T_0, or in practice, T_g. This effect is clearly illustrated for the case of $[C_4mim][N(CN)_2]$. Only data far above T_g can be included, and the calculated fragility m is much larger than any reported value in literature[35]. In addition the difference between T_0 and T_g is unrealistically small. Something similar applies to $[C_4mim]Cl$, although here m is more realistic. It has for sure the highest fragility of the compounds reported here.

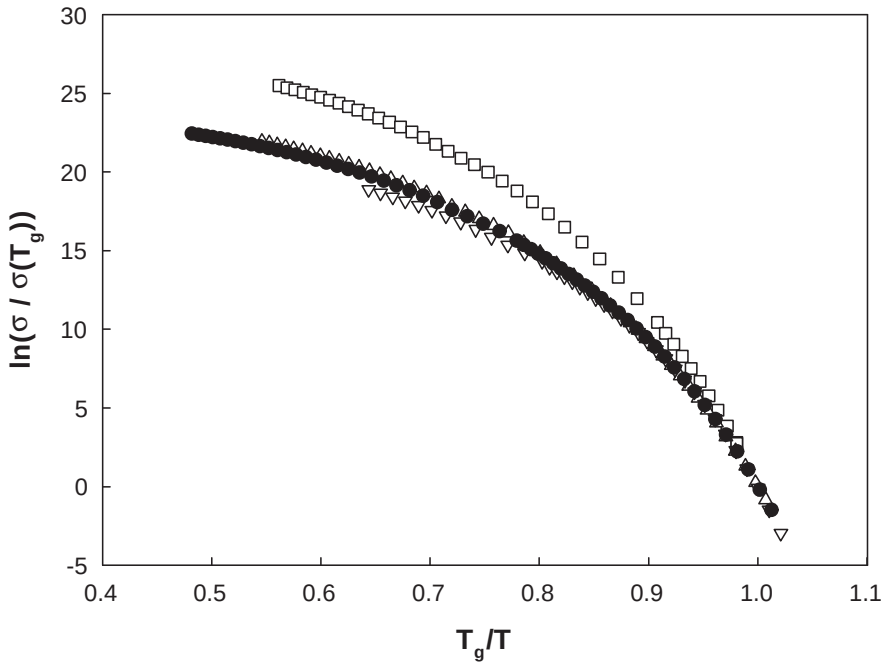

FIG. 2. T_g rescaled Arrhenius plot for the electrical conductivity versus inverse temperature for four of the ILs. □: [C_4mim]Br; △: [C_4mim]I, ▽: [C_4mim][NCS]; ●: [C_4mim][BF_4].

To verify the results obtained from the calculation, a plot was made were the temperatures are rescaled with T_g and the conductivities with $\sigma(T_g)$. The value for $\sigma(T_g)$ was obtained from the VFT fit. As a consequence, the curves for [C_4mim]Cl and [C_4mim][$N(CN)_2$] are not included, because for these compounds the procedure required an extensive extrapolation of the VFT fit, which could not be reliably made. Fig. 2 shows that of the four analyzed ILs [C_4mim]Br has the higher fragility, whereas the three other compounds have about the same curvature near T_g, consistent with the number obtained in Table III.

There are some tendencies that can be immediately assessed from the table and the figures:

- The electrical conductivity at room temperature is increasing with increasing anion size. This trend is reflected in the prefactor of the VFT expression, $\ln \sigma_\infty$.
- The fragility is decreasing with increasing anion size (larger m).
- T_g and T_0 are decreasing with increasing anion size.
- The VFT parameters and derived fragilities are not very different over the three temperature ranges (at least in those cases where all three ranges yield reliable numbers).

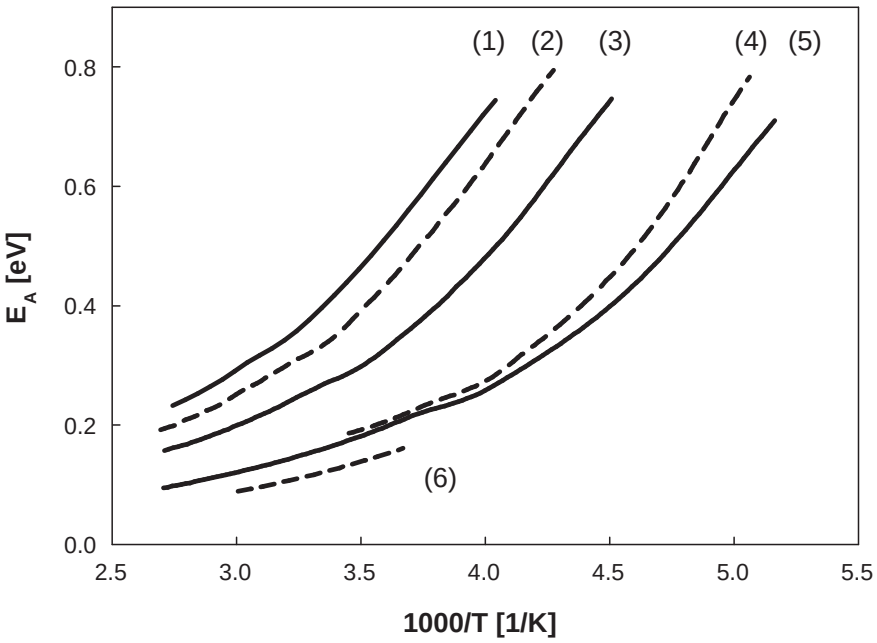

FIG. 3. Effective activation energy $E_A(T)$ as a function of inverse temperature. (1): $[C_4mim]Cl$; (2): $[C_4mim]Br$; (3): $[C_4mim]I$, (4): $[C_4mim][NCS]$; (5): $[C_4mim][BF_4]$; (6): $[C_4mim][N(CN)_2]$.

This suggests that a decoupling of the conductivity from the other physical parameters near T_g is not present in these systems.

As mentioned above, the extracted values for the fragility of the different compounds in Table III are subject to rather high uncertainties. This is a consequence of the definition of this quantity as a feature of the VFT curve in the neighbourhood of T_g, which could not be experimentally reached for all investigated ILs. Additionally the error on m also reflects the high uncertainty quoted for T_g.

C. Comparison between different models for the temperature dependence of the conductivity

Most researchers have been using the VFT equation to describe the temperature dependence of the relaxing physical quantities, but many other model functions have been proposed. In this Section, we shortly compare some of the models:

- the Adam–Gibbs equation[39]:

$$\sigma = \sigma_\infty \exp\left(-\frac{B'}{S_c(T)T}\right), \tag{5}$$

TABLE III. VFT fit parameters and derived quantities for the six ionic liquids.

Compound	σ_{RT} [S/m]	T_{low} [K]	T_{high} [K]	# data points	$\ln \sigma_\infty$ [S/m]		B [K]		T_0 [K]		T_g[l] [K]		m	
[C_4mim]Cl	0.0023	233	393[a]	92	8.1 ±	0.1	1626 ±	20	178.9±	0.6	205.1[g] ±	3	210 ±	50
		233	303[b]	44	10.7 ±	0.3	2076 ±	60	169 ±	1			142 ±	50
		233	267[c]	20	14 ±	1	2621 ±	200	159 ±	4			111 ±	30
[C_4mim]Br	0.0077	225	393	114	7.67±	0.06	1491 ±	10	175.4±	0.3	220.8[h] ±	2	69 ±	7
		225	298	63	9.1 ±	0.1	1723 ±	20	170.1±	0.5			64 ±	6
		225	287	54	9.7 ±	0.2	1804 ±	30	168.4±	0.7			63 ±	6
[C_4mim]I	0.028	213	393	118	7.03±	0.05	1343 ±	9	167.0±	0.2	214.7[i] ±	12	55 ±	30
		213	283	72[d]										
		213	279	69	8.4 ±	0.1	1532 ±	10	162.6±	0.2			53 ±	20
[C_4mim][NCS]	0.42	191	303	115	6.53±	0.02	1014 ±	3	156.0±	0.1	195.2 ±	7	56 ±	20
		191	243	81	6.79±	0.05	1041 ±	5	155.3±	0.1			55 ±	20
		191	253	87	6.69±	0.05	1031 ±	5	155.6±	0.1			56 ±	20
[C_4mim][$N(CN)_2$]	0.94	235	393	85	4.40±	0.03	523 ±	6	175.9±	0.5	184.6[j] ±	5	(556)[f] ±	700
		247	333	46	4.47±	0.03	528 ±	7	176.4±	0.7			(631)[f] ±	800
		235	240	/[e]										
[C_4mim][BF_4]	0.32	187	393	157	6.23±	0.03	1078 ±	6	149.7±	0.1	189.4[k] ±	13	56 ±	30
		187	273	105	6.86±	0.04	1160 ±	5	147.6±	0.1			55 ±	30
		187	233	72	7.24±	0.05	1205 ±	7	146.5±	0.2			54 ±	30

[a] Temperature range corresponding to the full liquid range.
[b] Temperature range corresponding to the range determined on the Stickel plot (see text for details).
[c] Temperature range between the lowest available value and $1.3T_g$.
[d] This range gives the same parameters as the next.
[e] This temperature range does not contain sufficient data points for a reliable fit.
[f] This value is not realistic, see text for details.
[g] Litt.: $T_g = 208$ K[3].
[h] Litt.: $T_g = 218.9$ K[36].
[i] Litt.: $T_g = 202$ K[20].
[j] Litt.: $T_g = 179$ K[37], $T_g = 183$ K[27].
[k] Litt.: $T_g = 190$ K[17], $T_g = 202$ K[38].
[l] The error on T_g has been determined from a comparison between our results and selected literature values. The difference between the values is the indicated error. For [C_4mim][NCS] the average of the other errors has been used.

where B' is an effective activation barrier and $S_c(T)$ the configurational entropy of the liquid;

- the Vogel–Fulcher–Tammann equation, given in Eq. (2), where the parameter B can be seen as the high temperature limit of the effective active activation energy;

- the MIGRATION-based expression applied by Šantić and co-workers[40]:

$$\sigma = \frac{\alpha}{T} \exp\left[-\frac{E^*}{k_B T} - \gamma \exp\left(\frac{E^*/K}{k_B T}\right)\right], \tag{6}$$

where E^* is the (Arrhenius-type) activation energy of the underlying process, for the other parameters we refer to Ref. 40;

- the expression that Mauro *et al.* recently[41] proposed:

$$\sigma = \sigma_\infty \exp\left[-\frac{K'}{T} \exp\left(\frac{C}{T}\right)\right], \tag{7}$$

where C is the (Arrhenius-type) activation energy of the underlying process that governs the configurational entropy and K' combines a number of constants related to the underlying model. A derivation and further references can be found in Ref. 41.

The two latter expressions, Eqs. (6) and (7), are representatives of a broader class of functions that contain an exponential function of $1/T$ as argument to another exponential function. Such functions typically emerge when the $B'/S_c(T)$ parameter of Eq. (5) is expanded based on some modelling of these parameters, or via a similar modification of the activation energy in the Arrhenius equation. In this respect, comparison of the results of such fits might give an indication of the validity of the underlying assumptions.

The results of fitting the experimental data with the different model functions are summarized in Fig. 3 for the Adam–Gibbs approach and in Table IV for the other models. For the fits we only used the three ILs for which the full temperature range from 120°C to T_g is available, and the fits were performed over this entire range. For the Adam–Gibbs approach, we will extend the discussion to all the ILs, because of the connection with the fragility m obtained in the previous section.

A first visual comparison of the residuals of the different fits does not show any important differences (Fig. 4). The χ^2 values, the sum of the squared deviations between the logarithmic values of σ from fit and experiment, are of the same order of magnitude. In order to compare

TABLE IV. Fit parameters for fits of the [C_4mim]Br, [C_4mim]I and [C_4mim][BF_4] conductivity data over the entire temperature range to Eqs. (2), (6) and (7). Parameters in parenthesis are kept fixed during the fitting. The number of digits printed is an indication for the obtained error on the parameters.

	VFT				Šantić *et al.*					Mauro *et al.*			
Compound	$\ln\sigma_\infty$	$B\cdot k_B$	T_0	χ^2	α	γ	E^*	K	χ^2	$\ln\sigma_\infty$	K	$C\cdot k_B$	χ^2
	[S/m]	[eV]	[K]		10^6 S· K/m		[eV]			[S/m]	[K]	[eV]	
[C_4mim]Br	7.67	0.128	175.4	0.0111	2.27	0.087	0.202	(1.9)	0.0033	3.69	157	0.070	0.0050
[C_4mim]I	7.03	0.116	167.0	0.0078	1.56	0.072	0.197	(1.9)	0.0033	3.39	144	0.066	0.0076
[C_4mim][BF_4]	6.23	0.093	149.7	0.0087	1.16	0.046	0.185	(1.9)	0.0017	3.16	119	0.059	0.0148

TABLE V. χ^2 ratios for the fits reported in Table IV

Compound	$\chi^2_{\text{Šantić}}/\chi^2_{\text{VFT}}$	$\chi^2_{\text{Mauro}}/\chi^2_{\text{VFT}}$	$\chi^2_{\text{Šantić}}/\chi^2_{\text{Mauro}}$
[C_4mim]Br	0.30	0.45	0.66
[C_4mim]I	0.42	0.97	0.43
[C_4mim][BF_4]	0.20	1.7	0.11

the fitting qualities, we have evaluated the ratios between the χ^2 values of the three models, and subjected these values to a statistical F-test. When the ratio lies between 0.74 en 1.35, then the fits can be considered equally good to a significance level of 95%. Ratios smaller than 1 indicate that the fit in the numerator is the better one. These ratios are given in Table V. The VFT and the model of Mauro *et al.* perform about the same, and both are worse than the model of Šantić *et al.*. It is important to mention that this function has an extra parameter compared to the VFT and the Mauro *et al.* function.

For a good theoretical model, besides giving a good fit for a single compound, meaningful evolutions should be visible in the parameters when series of compounds are measured. The prefactors for the three models show a decrease from [C_4mim]Br towards [C_4mim][BF_4]. Also the "fundamental activation energy" parameters in the model functions (i.e. B, E^* and C in the VFT, Šantić and Mauro model respectively) show a decrease in the same direction (the direction of decreasing anion-cation interaction). Also the other parameters reported

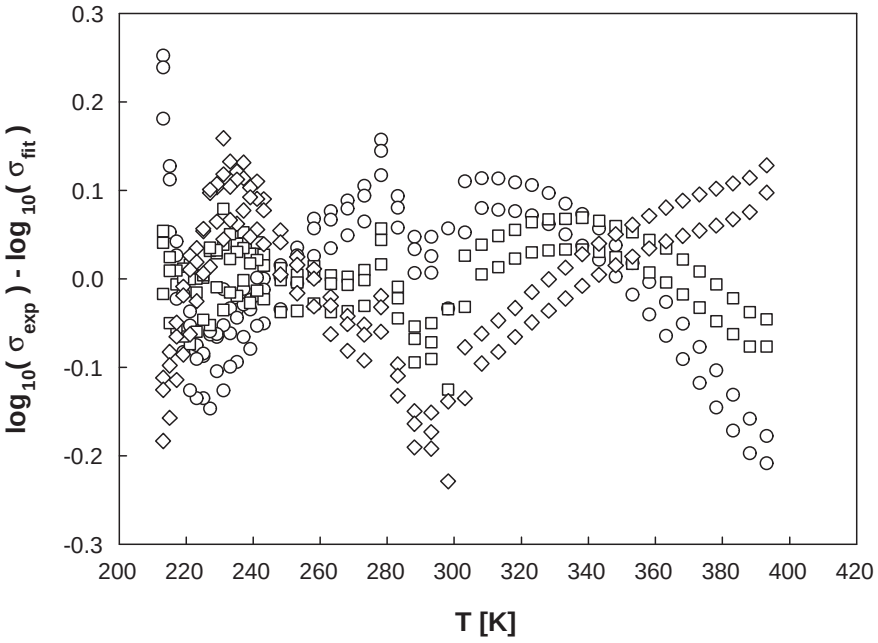

FIG. 4. Residuals of the fits of $\log \sigma$ to the different model functions for $[C_4mim]I$. ○: VFT fit; □: Šantić *et al.* fit; ◇: Mauro *et al.* fit.

show a systematic dependence. It should be mentioned that the parameter K of the Šantić *et al.* approach was kept fixed during the fit to the literature value[40] for $[C_4mim][BF_4]$. When this parameter is left free, small changes in K lead to substantial changes in the other parameters, breaking down the systematic evolutions that are seen with K fixed. It this respect, the separate determination of K from a different approach as described in Ref. 40 appears to be required for a succesfull application of this method. Thus all three functions allow the researcher to obtain parameter values that reflect the physics of systematic series of compounds, with the caveat for the function of Šantić *et al.* to be kept in mind.

Hence the comparison between the VFT, Šantić and Mauro functions does not give a decisive argument to prefer or exclude one of these respective models. A similar conclusion concerning the VFT and the Mauro *et al.* model was reached on a broader data set[42]: while in many cases the Mauro *et al.* model performed better than the VFT function, several examples of the opposite were found too.

The formulation of the Adam–Gibbs approach above leads to a description in terms of the function $S_c(T)$, rather than a limited set of fit parameters. As such, the "fit" cannot be quantified and discussed as above, but the discussion will be based on Fig. 3, where $E_A(T)$

is plotted, essentially a rescaling of $B'/S_c(T)$:

$$E_A(T) = k_B \frac{\partial \log_{10} \sigma^{-1}}{\partial(1/T)} = \frac{k_B}{\ln 10} \frac{B'}{S_c(T)} \tag{8}$$

Note that $E_A(T_g)/(k_B T_g)$ corresponds to the fragility m. An expression for the fragility can also be obtained from the Šantić *et al.* and the Mauro *et al.* models following the definition in Eq. 4. For both models, the tendency earlier observed for the fragility derived from the VFT equation is reproduced, but with slightly different absolute values.

Towards high temperatures the effective activation energies of the different anions tend to the same value. This is expected since in the high temperature limit the thermal energy starts to be so high that the details of the inter-ionic potentials become less important. On the other hand, the low temperature value effective activation energy is strongly dependent on the ion size: the change of activation energy with temperature, which reflects the strength of the curvature of the Arrhenius plot, decreases as the size of anion is increasing from Cl^-, over Br^- and I^- towards $[NCS]^-$, $[N(CN)_2]^-$ and $[BF_4]^-$. This trend is consistent with the decreasing trend of the m values in Table III.

For the three ILs that we discuss here, the values of $E_A(T)$ are decreasing with increasing ion size, the same tendency as for the related fit parameters in the three discussed fit models. This tendency also holds in case the temperatures are rescaled towards T_g, i.e. comparing values of $E_A(T)$ at the same distance of T_g, as opposed to comparing towards the available thermal energy in the previous case, the latter being probably the more natural.

In summary, all approaches show essentially an increasing value of the effective activation energywith suspected increasing anion-cation interaction. This feature will be discussed in more detail below in terms of the energy landscape model.

IV. DISCUSSION

In the previous analysis, the potential effects of changes in the ionicity of the ionic liquid have been ignored. A thorough discussion of this subject would require additional data. Examples of such analysis can be found in Refs. 6,7,17–19,43–45, where a comparison of self-diffusion data with conductivity and/or viscosity data yields interesting conclusions on the presence and influence of ion pairs and related phenomena.

A very general way to describe the relation between conductivity and molecular mobility

in ILs is

$$\sigma(T) = \sum_i n_i^+(T) q_i^+ \mu_i^+(T) + \sum_j n_j^-(T) q_j^- \mu_j^-(T) \ , \tag{9}$$

where n is the number density of charge carriers, q the charge of a carrier and μ the mobility of the charge carrier, for positive (index +) and negative carriers (index −), and for different charge carrier types (indices i and j). In the following discussion, the relation will be simplified under certain assumptions.

- Only singly charged carriers are present: $q^+ = q^- = e = 1.6 \cdot 10^{-19}$ C.
- The charge carriers are the cation and the anion.
- The number density of anion and cation are the same. This corresponds to assuming a macroscopically neutral liquid.
- The molecular mobilities for anion and cation are the same.

From pulsed field gradient NMR measurements, it is known that this last assumption is not entirely true[17–19,43–46]: in many cases the cation seems to be slightly more mobile than the anion. However, since the temperature dependencies of the mobilities are the same, this can be resolved by introducing an averaged mobility. Thus the previous equation is simplified to

$$\sigma(T) = n(T) e \mu(T) \ . \tag{10}$$

In this equation still two separate temperature dependencies arise that contribute to that of $\sigma(T)$. Changes in the number density $n(T)$ are related to changes in the amount of free ions that can carry charge around through the IL (i.e. free ions versus ions pairs), and this quantity has been shown to be only weakly temperature dependent[6,7,45].

Hence, we do not think that changes in ionicity have an important influence on our analysis, in the sense that the effect of temperature and ionic details on the behavior of the electrical conductivity can be interpreted as dominantly due to the effect on the ionic mobility. Even if they have, the electrical conductivity in itself is an important quantity in ILs in its own right.

Models based on the theory of Brownian motion lead to the Walden rule[47,48], which predicts an inverse proportionality between the molar conductivity Λ and the viscosity η:

$$\Lambda \eta = \text{const} \ . \tag{11}$$

The constant is essentially a material constant that increases with increasing ionic radius r. The validity of the Walden rule has been shown for ILs[48].

The approach to interpreting the conductivity data and their link to the molecular diffusion via such relations as the Walden rule, the Stokes–Einstein equation and the Einstein–Smoluchowski equation has been used before, generally confirming its validity. Particularly interesting work in this context, already indicated above, has been done by Tokuda and co-workers[17–19,43] and Sangoro and co-workers[6,7], who used a combination of pulsed field gradient NMR (allowing to determine the self-diffusion coefficients) and electrical conductivity measurements. Tokuda *et al.* were able, by the use of fluorinated anions, to selectively determine the diffusion coefficients for the anion and the cation seperately. Also noteworthy is the extensive combined analysis of Stolwijk and Obeidi[45].

When, based on the observations above, we attempt to predict the electrical conductivity for a series of ILs in which the size of the anion is increasing, we arrive at the conclusion that, for an increasing ionic radius r, the mobility is decreasing and as a direct consequence also that σ is decreasing. This is the opposite tendency compared to what is observed in the actual measurement. There are, in our view, two main interactions that are counteracting the expected decreasing molecular mobility with increasing ionic size: hydrogen bonding and charge delocalization.

First, we selected these ionic liquids based on their hydrogen bonding ability. It is known that hydrogen bonds can be formed between the hydrogen atoms on the imidazolium ring and a halide ion[49,50]. Due to increased charge delocalization, the strength of this hydrogen bond decreases if the halide ion becomes larger. The decrease of the hydrogen bond strength can be interpreted as a decreasing interaction of the charge carrier with its environment and thus to an increase in molecular mobility and conductivity.

The second effect acting on the effective viscosity is that when the ion becomes larger, the charge is effectively more spread over the surface of the ion, reducing the charge surface density, and thus decreasing Coulomb interaction. In the same way as for the hydrogen bond, such decreasing interionic interaction ultimately increases the conducitivity.

In this particular series, the "secondary effects" of the increasing anion size (decreased hydrogen bond and Coulomb interaction) have a much stronger influence on the molecular mobility than the "primary effect", the (*a priori* expected) decrease of mobility for larger ions. Also, by fixing the cation in the investigated IL series, changes in the van der Waals

forces are kept to a minimum. In previous work[18,20,21,25] it was shown that an increasing length of the alkyl chain attached to the cation head has an overall decreasing effect on σ and an increasing one on the viscosity. This decrease of molecular mobility was explained by the increased van der Waals forces keeping the chains together, thus immobilizing them, and by the increased steric hindrance and molecular mass and inertia.

For explaining the tendency of increasing electric conductivity and decreasing fragility with increasing anion size we make use of the conceptual picture of conduction as an activated process, probing the potential energy landscape[51] whose morphology depends on the detailed molecular interactions. On a microscopic level, at low temperatures, the positions and mobility of ions are determined by rather strong Coulomb, hydrogen bond and van der Waals forces, and ions are rather strongly hindered to move away from their metastable equilibrium states. The occupied conformational states are located in the deep and steep parts of the potential energy valleys and conformational changes (necessary for conduction and reorientation) require high activation energies. With increasing temperature, higher energy states are occupied that are on average further away from the steep and rigid valleys, and thus the activation energy becomes typically smaller. The molecular mobility is enhanced, and the viscous hindrance against conduction and reorientation is reduced.

In this picture, it is clear that with increasing anion size, since the ionic charge distributions are less strongly localized, the potential energy valleys become smoother, thus reducing the low temperature activation energy. This is consistent with the experimental observation that ILs with larger anion size show a weaker temperature dependence of their activation energy (Fig. 3), thus a smaller fragility. Also, the effect reduced interaction strength of larger ions due to the more extended spread of the charge distribution is consistent with an increased mobility, in spite of their enhanced mass.

V. CONCLUSION

We have studied the electrical conductivity of a series of six imidazolium ionic liquids over a broad temperature range towards their glass transition temperature. In the series, the cation was fixed, while the anion was varied in size and hydrogen bonding ability. The measurements show that the electrical conductivity is increasing with increasing ion size. The fragility decreases with increasing anion size. This effect is confirmed by the anion size

dependence of other, more robust curve features that reflect the curvature of the Arrhenius plot, such as the degree of temperature dependence of the effective activation energy.

The decrease of the interaction between the anion and the cation with increasing anion size —because of reduced hydrogen bond strength and of reduced Coulomb interaction— can be used to explain both observations. In spite of the larger anion mass, the reduced interionic interaction leads to a higher mobility, resulting in an increased electric conductivity. Similarly, within the potential energy landscape interpretation of the glass transition, the reduced interaction for larger anions leads to a potential energy landscape with less steep potential energy wells, resulting in a lower effective activation energy at low temperatures.

ACKNOWLEDGMENTS

This research is supported by IDO/05/005, "Ionic liquids as medium for catalytic reactions and electrodeposition of metal layers", K.U.Leuven; by Tournesol exchange project T2006.05 between K.U.Leuven, Belgium and Univ. Littoral, Dunkerque, France; by FWO-V, Belgium project G.0230.07 ("AVISCO") and by GOA/2007/06/ project, K.U.Leuven. J.L. acknowledges the Research Fund of K.U.Leuven for a postdoctoral fellowship (PDM/07/098). Support by Iolitec (Denzlingen, Germany) is greatly appreciated. The authors thank M. Wübbenhorst for assistance in the analysis of the conductivity data.

REFERENCES

[1]E. W. Castner, Jr. and J. F. Wishart, "Spotlight on ionic liquids," J. Chem. Phys., **132**, 120901 (2010).

[2]A. Rivera and E. A. Rössler, "Evidence of secondary relaxations in the dielectric spectra of ionic liquids," Phys. Rev. B, **73**, 212201 (2006).

[3]A. Rivera, A. Brodin, A. Pugachev, and E. A. Rössler, "Orientational and translational dynamics in room temperature ionic liquids," J. Chem. Phys., **126**, 114503 (2007).

[4]O. Russina, M. Beiner, C. Pappas, M. Russina, V. Arrighi, T. Unruh, C. L. Mullan, C. Hardacre, and A. Triolo, "Temperature dependence of the primary relaxation in 1-hexyl-3-methylimidazolium bis{(trifluoromethyl)sulfonyl}imide," J. Chem. Phys. B, **113**, 8469 (2009).

[5]N. Ito and R. Richert, "Solvation dynamics and electric field relaxation in an imidazolium-PF_6 ionic liquid: From room temperature to the glass transition," J. Phys. Chem. B, **111**, 5016 (2007).

[6]J. R. Sangoro, A. Serghei, S. Naumov, P. Galvosas, J. Kärger, J. Wespe, F. Bordusa, and F. Kremer, "Charge transport and mass transport in imidazolium-based ionic liquids," Phys. Rev. E, **77**, 051202 (2008).

[7]J. Sangoro, C. Iacob, A. Serghei, S. Naumov, P. Galvosas, J. Kärger, C. Wespe, F. Bordusa, A. Stoppa, J. Hunger, R. Buchner, and F. Kremer, "Electrical conductivity and translational diffusion in the 1-butyl-3-methylimidazolium tetrafluoroborate ionic liquid," J. Chem. Phys., **128**, 214509 (2008).

[8]A. Triolo, O. Russina, H.-J. Bleif, and E. Di Cola, "Nanoscale segregation in room temperature ionic liquids," J. Phys. Chem. B, **111**, 4641 (2007).

[9]A. Triolo, A. Mandanici, O. Russina, V. Rodriguez-Mora, M. Cutroni, C. Hardacre, M. Nieuwenhuyzen, H.-J. Bleif, L. Keller, and M. A. Ramos, "Thermodynamics, structure, and dynamics in room temperature ionic liquids: The case of 1-butyl-3-methyl imidazolium hexafluorophosphate ([bmim][PF_6])," J. Phys. Chem. B, **110**, 21357 (2006).

[10]W. Xu, L.-M. Wang, R. A. Nieman, and C. A. Angell, "Ionic liquids of chelated orthoborates as model ionic glassformers," J. Phys. Chem. B, **107**, 11749 (2003).

[11]W. Xu, E. I. Cooper, and C. A. Angell, "Ionic liquids: Ion mobilities, glass temperatures, and fragilities," J. Phys. Chem. B, **107**, 6170 (2003).

[12]M. Yoshizawa, W. Xu, and C. A. Angell, "Ionic liquids by proton transfer: Vapor pressure, conductivity, and the relevance of $\Delta \mathrm{p}K_a$ from aqueous solutions," J. Am. Chem. Soc., **125**, 15411 (2003).

[13]J.-P. Belieres and C. A. Angell, "Protic ionic liquids: Preparation, characterization, and proton free energy level representation," J. Phys. Chem. B, **111**, 4926 (2007).

[14]H. Markusson, J.-P. Beliéres, P. Johansson, C. A. Angell, and P. Jacobsson, "Prediction of macroscopic properties of protic ionic liquids by ab initio calculations," J. Phys. Chem. A, **111**, 8717 (2007).

[15]T. L. Greaves, A. Weerawardena, C. Fong, I. Krodkiewska, and C. J. Drummond, "Protic ionic liquids: Solvents with tunable phase behavior and physicochemical properties," J. Phys. Chem. B, **110**, 22479 (2006).

[16]M. Anouti, M. Caillon-Caravanier, C. Le Floch, and D. Lemordant, "Alkylammonium-

based protic ionic liquids. II. ionic transport and heat-transfer properties: Fragility and ionicity rule," J. Phys. Chem. B, **112**, 9412 (2008).

[17]H. Tokuda, K. Hayamizu, K. Ishii, M. A. B. H. Susan, and M. Watanabe, "Physicochemical properties and structures of room temperature ionic liquids. 1. variation of anionic species," J. Phys. Chem. B, **108**, 16593 (2004).

[18]H. Tokuda, K. Hayamizu, K. Ishii, M. A. B. H. Susan, and M. Watanabe, "Physicochemical properties and structures of room temperature ionic liquids. 2. variation of alkyl chain length in imidazolium cation," J. Phys. Chem. B, **109**, 6103 (2005).

[19]H. Tokuda, K. Ishii, M. A. B. H. Susan, S. Tsuzuki, K. Hayamizu, and M. Watanabe, "Physicochemical properties and structures of room temperature ionic liquids. 3. variation of cationic structures," J. Phys. Chem. B, **110**, 2833 (2006).

[20]H. A. Every, A. G. Bishop, D. R. MacFarlane, G. Orädd, and M. Forsyth, "Transport properties in a family of dialkylimidazolium ionic liquids," Phys. Chem. Chem. Phys., **6**, 1758 (2004).

[21]J. Leys, M. Wübbenhorst, C. P. Menon, R. Rajesh, J. Thoen, C. Glorieux, P. Nockemann, B. Thijs, K. Binnemans, and S. Longuemart, "Temperature dependence of the electrical conductivity of imidazolium ionic liquids," J. Chem. Phys., **128**, 064509 (2008).

[22]"`http://www.basionics.com/en/ionic-liquids/products/data/st70.htm`," (May 2010).

[23]J. G. Huddleston, A. E. Visser, W. M. Reichert, H. D. Willauer, G. A. Broker, and R. D. Rogers, "Characterization and comparison of hydrophilic and hydrophobic room temperature ionic liquids incorporating the imidazolium cation," Green Chem., **3**, 156 (2001).

[24]"`http://www.basionics.com/en/ionic-liquids/products/data/vs02.htm`," (May 2010).

[25]Y. Yoshida, O. Baba, and G. Saito, "Ionic liquids based on dicyanamide anion: Influence of structural variations in cationic structures on ionic conductivity," J. Phys. Chem. B, **111**, 4742 (2007).

[26]T. Nishida, Y. Tashiro, and M. Yamamoto, "Physical and electrochemical properties of 1-alkyl-3-methylimidazolium tetrafluoroborate for electrolyte," J. Fluorine Chem., **120**, 135 (2003).

[27]C. P. Fredlake, J. M. Crosthwaite, D. G. Hert, S. N. V. K. Aki, and J. F. Brennecke,

"Thermophysical properties of imidazolium-based ionic liquids," J. Chem. Eng. Data, **49**, 954 (2004).

[28]E. Donth, *The Glass Transition: Relaxation Dynamics in Liquids and Disordered Materials* (Springer Verlag, Berlin, 2001).

[29]F. Stickel, E. W. Fischer, and R. Richert, "Dynamics of glass-forming liquids. I. temperature-derivative analysis of dielectric relaxation data," J. Chem. Phys., **102**, 6251 (1995).

[30]W. Götze and L. Sjögren, "Relaxation processes in supercooled liquids," Rep. Prog. Phys., **55**, 241 (1992).

[31]H. Sillescu, "Heterogeneity at the glass transition: a review," J. Non-Cryst. Solids, **243**, 81 (1999).

[32]M. D. Ediger, "Spatially heterogeneous dynamics in supercooled liquids," Annu. Rev. Phys. Chem., **51**, 99 (2000).

[33]R. Böhmer, K. L. Ngai, C. A. Angell, and D. J. Plazek, "Nonexponential relaxations in strong and fragile glass formers," J. Chem. Phys., **99**, 4201 (1993).

[34]D. D. Jackson, "Most squares inversion," J. Geophys. Res., **81**, 1027 (1976).

[35]Q. Qin and G. B. McKenna, "Correlation between dynamic fragility and glass transition temperature for different classes of glass forming liquids," J. Non-Cryst. Solids, **352**, 2977 (2006).

[36]Y. U. Paulechka, G. J. Kabo, A. V. Blokhin, A. S. Shaplov, L. E. I., and Y. Vygodskii, "Thermodynamic properties of 1-alkyl-3-methylimidazolium bromide ionic liquids," J. Chem. Thermodyn., **39**, 158 (2007).

[37]Y. Yoshida, O. Baba, C. Larriba, and G. Saito, "Imidazolium-based ionic liquids formed with dicyanamide anion: Influence of cationic structure on ionic conductivity," J. Phys. Chem. B, **111**, 12204 (2007).

[38]J. D. Holbrey and K. R. Seddon, "The phase behaviour of 1-alkyl-3-methylimidazolium tetrafluoroborates; ionic liquids and ionic liquid crystals," J. Chem. Soc., Dalton Trans., 2133 (1999).

[39]G. Adam and J. H. Gibbs, "On the temperature dependence of cooperative relaxation properties in glass forming liquids." J. Chem. Phys., **43**, 139 (1965).

[40]Š. Ana, W. Wrobel, M. Mutke, R. D. Banhatti, and K. Funke, "Frequency-dependent fluidity and conductivity of an ionic liquid," Phys. Chem. Chem. Phys., **11**, 5930 (2009).

[41]J. C. Mauro, Y. Yue, A. J. Ellison, P. K. Gupta, and D. C. Allan, "Viscosity of glass-forming liquids," Proc. Natl. Acad. Sci. USA, **106**, 19780 (2009).

[42]P. Lunkenheimer, S. Kastner, M. Köhler, and A. Loidl, "Temperature development of glassy α-relaxation dynamics determined by broadband dielectric spectroscopy," arXiv:1004.5137 (2010).

[43]H. Tokuda, S. Tsuzuki, M. A. B. H. Susan, K. Hayamizu, and M. Watanabe, "How ionic are room-temperature ionic liquids? an indicator of the physicochemical properties," J. Phys. Chem. B, **110**, 19593 (2006).

[44]A. Noda, K. Hayamizu, and M. Watanabe, "Pulsed-gradient spin-echo ^{1}H and ^{19}F NMR ionic diffusion coefficient, viscosity, and ionic conductivity of non-chloroaluminate room-temperature ionic liquids," J. Phys. Chem. B, **105**, 4603 (2001).

[45]N. Stolwijk and S. Obeidi, "Combined analysis of self-diffusion, conductivity, and viscosity data on room temperature ionic liquids," Electrochimica Acta, **54**, 1645 (2009).

[46]S. H. Chung, R. Lopato, S. G. Greenbaum, H. Shirota, E. W. Castner, and J. F. Wishart, "Nuclear magnetic resonance study of the dynamics of imidazolium ionic liquids with -$CH_2Si(CH_3)_3$ vs -$CH_2C(CH_3)_3$ substituents," J. Phys. Chem. B, **111**, 4885 (2007).

[47]C. Rey-Castro and L. F. Vega, "Transport properties of the ionic liquid 1-ethyl-3-methylimidazolium chloride from equilibrium molecular dynamics simulation. the effect of temperature," J. Phys. Chem. B, **110**, 14426 (2006).

[48]P. Wasserscheid and T. Welton, eds., *Ionic Liquids in Synthesis* (Wiley-VCH Verlag, Weinheim, Germany, 2003).

[49]A. G. Avent, P. A. Chaloner, M. P. Day, K. R. Seddon, and T. Welton, "Evidence for hydrogen bonding in solutions of 1-ethyl-3-methylimidazolium halides, and its implications for room-temperature halogenoaluminate(III) ionic liquids," J. Chem. Soc., Dalton Trans., 3405 (1994).

[50]A. Elaiwi, P. B. Hitchcock, K. R. Seddon, N. Srinivasan, Y.-M. Tan, T. Welton, and J. A. Zora, "Hydrogen bonding in imidazolium salts and its implications for ambient-temperature halogenoaluminate(III) ionic liquids," J. Chem. Soc., Dalton Trans., 3467 (1995).

[51]P. G. Debenedetti and F. H. Stillinger, "Supercooled liquids and the glass transition," Nature, **410**, 259 (2001).

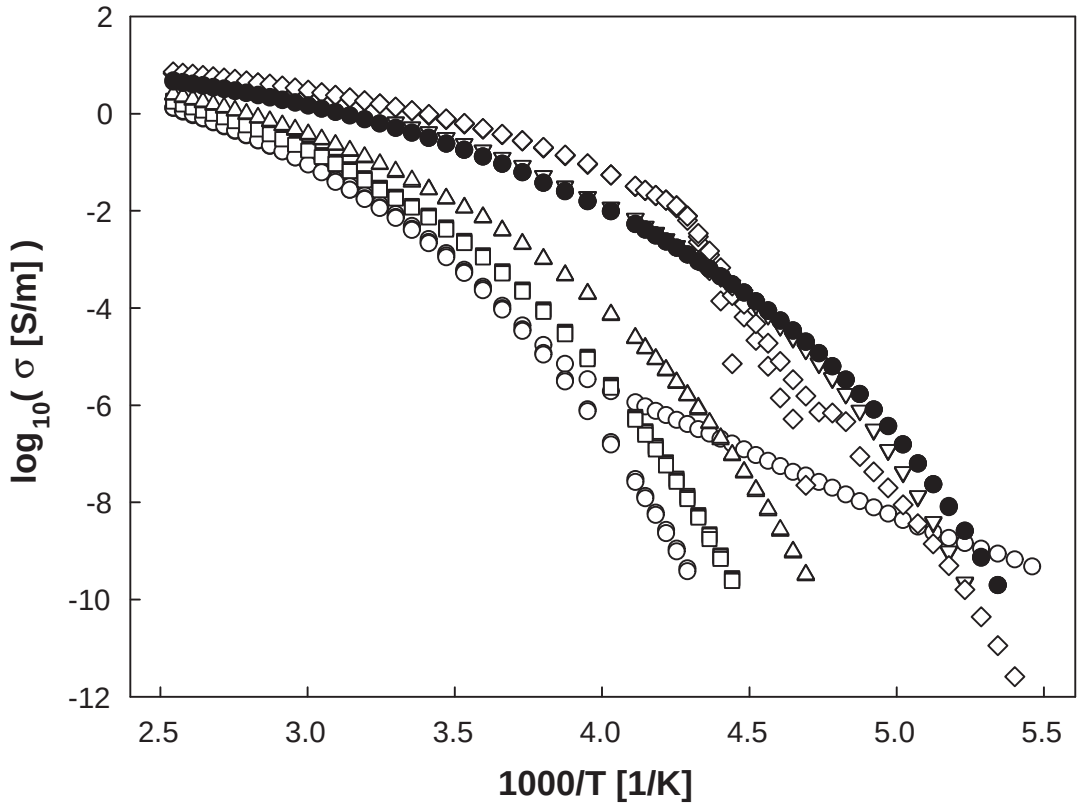
2
0
-2
-4
-6
-8
-10
-12
2.5
3.0
3.5
4.0
4.5
5.0
5.5
log10(σ [S/m])
1000/T [1/K]

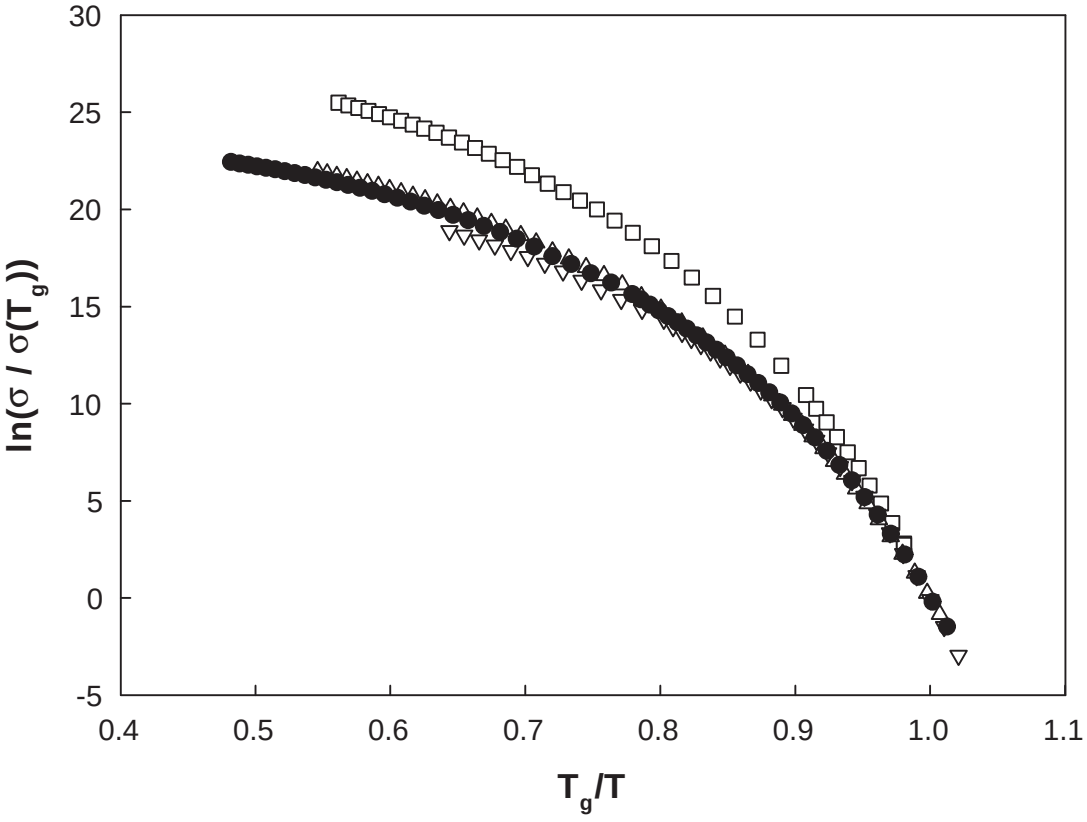
30
25
20
15
10
5
0
-5
0.4
0.5
0.6
0.7
0.8
0.9
1.0
1.1
ln(σ / σ(T_g))
T_g/T

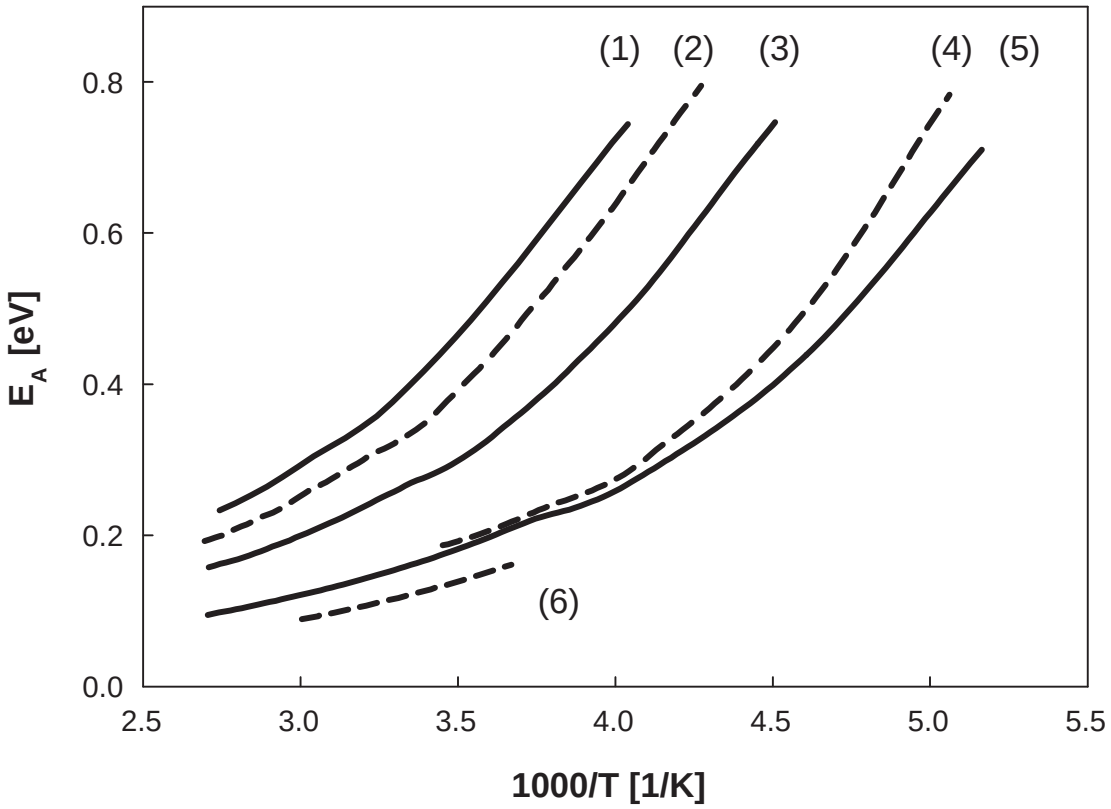
(1)
(2)
(3)
(4)
(5)
(6)
0.0
0.2
0.4
0.6
0.8
2.5
3.0
3.5
4.0
4.5
5.0
5.5
E_A [eV]
1000/T [1/K]

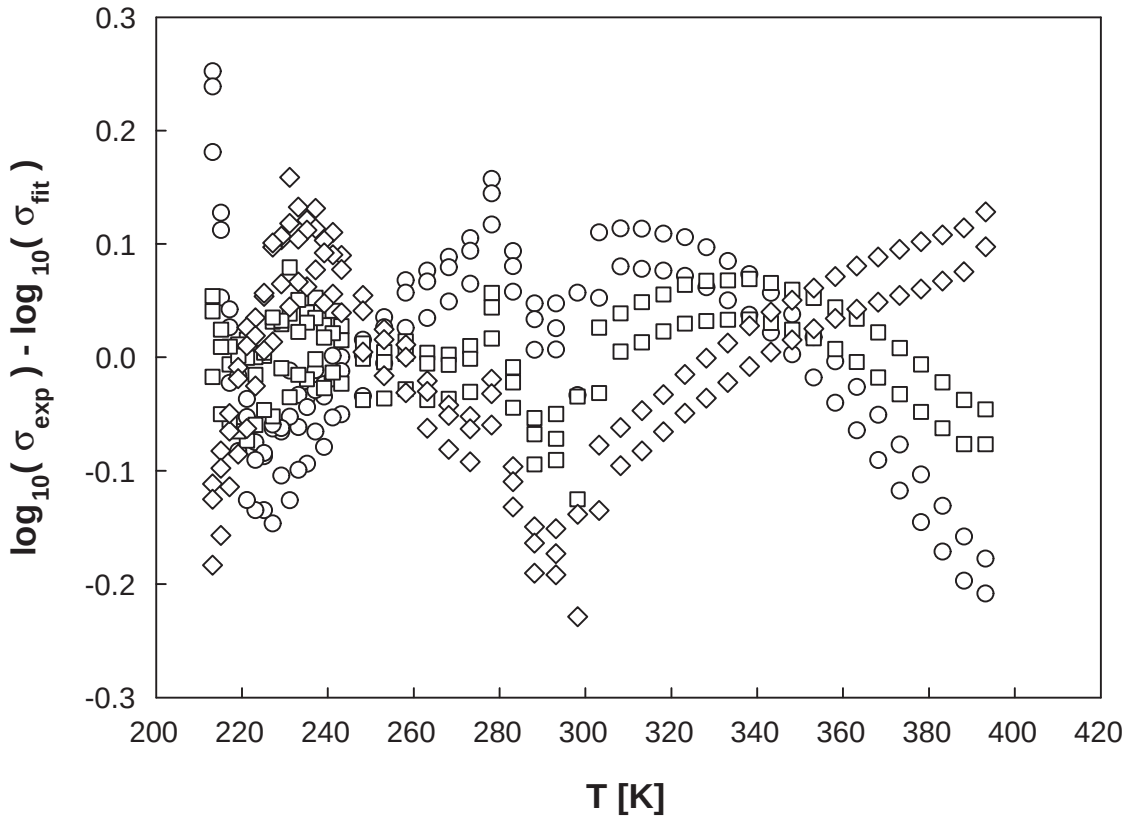
0.3
0.2
0.1
0.0
-0.1
-0.2
-0.3
200
220
240
260
280
300
320
340
360
380
400
420
log10(σexp) - log10(σfit)
T [K]